Journal of Materials Chemistry C

ROYAL SOCIETY OF CHEMISTRY

PAPER

View Article Online
View Journal | View Issue

Cite this: J. Mater. Chem. C, 2024, 12, 11594

Facile fabrication of dual-conductivity, humidity-responsive single-layer membranes: towards advanced applications in sensing, actuation, and energy generation†

Ioanna Tzoumani,*[a] Denisa Druvari,[a] Konstantinos C. Andrikopoulos,[a] Antonio Dominguez-Alfaro,[b] George G. Malliaras[b] and Joannis K. Kallitsis*[ac]

Humidity sensors and actuators have recently gained significant attention, largely owing to their broad applicability in innovative fields. This study presents the fabrication of smart single-layer membranes with mixed conductivity and high responsiveness to humidity. Utilizing a water-based processing method, partially-carboxylated multi-walled carbon nanotubes (CNTs-COOH) were incorporated into flexible cross-linked composite membranes, alongside sodium poly(4-styrene sulfonate-*co*-glycidyl methacrylate) (P(SSNa-*co*-GMA40)) and polyacrylic acid (PAA). This approach led to membranes with mixed conductivity, where CNTs were employed for electronic conductivity and P(SSNa-*co*-GMA40) provided ionic conductivity and humidity responsiveness. The developed membranes were thoroughly studied, in terms of microstructure morphology, physicochemical, mechanical and humidity sensing properties, while an extensive conductivity study was conducted as well. These smart composite membranes with responsive humidity-driven deformation show potential applications such as non-contact switches or soft-robotics materials. Furthermore, membranes with 30 wt% CNTs are considered an effective hygroelectric generator, providing an environmentally friendly and cost-effective new approach for moisture electricity generators (MEGs).

Received 28th May 2024,
Accepted 28th June 2024

DOI: 10.1039/d4tc02195a

rsc.li/materials-c

Introduction

A novel category of intelligent responsive actuators has emerged,[1] showcasing the ability to directly convert various environmental stimuli, such as heat, temperature, light, electricity, and humidity, into mechanical movements without the need for an energy supply system. These innovative materials have found significant applications in diverse fields,[2–5] including soft robotics,[6–8] wearable electronics,[9–12] environment-triggered sensors,[13,14] health monitoring,[15–17] non-contact switches[18,19] and power generation.[20] Among them there has been enormous interest in humidity-driven actuators since wet gases, such as water vapors or humidity in the atmosphere, can be employed as a huge renewable source for energy conversion with minimal environmental impact.

In general, the design of humidity-sensitive actuators relies on the utility of functional materials with varying hydrophilic capacities responding to gradient humidity through asymmetric deformation. Specifically, hydrophilic groups, such as –OH, –COOH and –SO_3H, present high affinity with water molecules and cause the actuator to expand through a swelling mechanism, whereas less hydrophilic/hydrophobic components promote de-swelling of the actuator through desorption of water molecules.[21] Commonly used materials in humidity actuators include metal oxides, ceramics, polymers, semiconductors, and carbon materials.[22] Regarding their morphology, humidity-responsive actuators typically involve a bilayer/multilayer structure that combines an active material layer sensitive to humidity with a passive material layer inert to humidity.[23,24] However, common limitations persist, including limited response range, low sensitivity, interlayer delamination, poor robustness, and a complex construction process, hindering the broader application of humidity-responsive actuators. To tackle these challenges, significant efforts have recently been directed towards the design and fabrication of single-layer humidity-responsive actuators made from homogeneous composite

[a] Department of Chemistry, University of Patras, GR-26504, Patras, Greece. E-mail: tzoumani@ac.upatras.gr, kallitsi@upatras.gr
[b] Electrical Engineering Division, Department of Engineering, University of Cambridge, Cambridge, UK
[c] Foundation for Research and Technology-Hellas, Institute of Chemical Engineering Sciences (FORTH/ICE-HT), Stadiou Str., GR-26504, Rio-Patras, Greece

† Electronic supplementary information (ESI) available: Detailed materials & methods, additional experimental data including tables, figures and movies. See DOI: https://doi.org/10.1039/d4tc02195a

materials.[25–27] These materials exhibit good actuation stability even after repeated deformation, but they often have a slow response speed. A suggested solution is the incorporation of nano-channels to the structures to enhance water flow permeability, facilitating both responsiveness and recovery of the actuator to both wet and dry stimuli.[28]

Carbon nanotubes (CNTs) are highly versatile materials with unique properties *e.g.* high elastic modulus, mechanical strength, and high electrical conductivity[29–31] that renders them appealing for the creation of composite materials with diverse potential applications.[32,33] However, the intrinsic hydrophobic nature of CNTs and agglomeration caused by van der Waals forces pose limitations to their utilization in humidity sensing application. Recent efforts have focused on enhancing the sensitivity of CNT-based humidity materials including surface modification treatments and blending CNTs with hydrophilic polymers.[34,35] These modifications along with the high aspect ratio and nanoscale hollow structure of CNTs make them ideal candidates for constructing resistive-type humidity sensors.[36]

Humidity-sensitive materials that can generate electricity directly from their interaction with moisture have been lately utilized for the creation of a new range of self-powered devices.[20] As a highly innovative technology, moisture electricity generators (MEGs) offer a new way of generating electricity by harvesting energy from moisture, derived from the interactions between water molecules and hydrophilic functional groups.[37] Such materials can find potential applications in self-powered electronics, healthcare, information storage and wearable electronics.[38,39] As a result, the development of self-powered flexible sensors is of utmost significance.

In this study, we introduce a facile design for a crosslinked single-layer membrane comprising a hydrophilic polymer system integrated with partially carboxylated carbon nanotubes (CNTs). The fabrication process of this membrane is very facile, cost-effective, scalable, and environmentally friendly, requiring aqueous mild conditions and low CNTs content (5–30% w/w). The polymeric/CNTs composite possesses excellent water absorption/desorption capabilities, while the polymeric structure of P(SSNa-*co*-GMA40)/PAA exhibits hydrophilic properties, whereas the CNTs component exhibits hydrophobic properties. These self-standing single-layer composite membranes combine ionic conductivity from the matrix and electronic conductivity from the dispersed CNTs, providing the characteristics needed for intelligent materials in non-contact human–machine interface applications such as smart switches or health monitoring systems. Moreover, these flexible, self-standing membranes offer great opportunity in the field of soft robotics (gripper robot), presenting spontaneous and continuous motility under gradient humidity as well as in moisture-driven electricity generation.

Results and discussion

Preparation of polymer/CNTs composite membranes

A schematic illustration for the preparation of the humidity-responsive P(SSNa-*co*-GMA40)/PAA/CNTs composite membranes is depicted in Fig. 1. The whole process is facile and scalable while maintaining an environmentally friendly character through its water-based methodology. First, carboxylated CNTs with a diameter of 30–50 nm were added in the aqueous solution of P(SSNa-*co*-GMA40) at ratios of 5, 10, 20 or 30 wt% with respect to the polymer. The suspension formed is homogeneous and stable (Fig. S1, ESI†), as evidenced by the absence of precipitation after 1 month under ambient conditions. Afterwards, the CNTs dispersion was mixed with an aqueous solution of PAA homopolymer to enhance the stability of the final membrane through a crosslinking reaction of the active carboxyl groups with epoxide group of GMA unit in the P(SSNa-*co*-GMA40) copolymer, as reported in previous studies.[40,41] In this work, partially carboxylated CNTs are employed to increase the humidity responsiveness/recovery of the resulting material by forming a porous network structure that is expected to facilitate water transport through the membrane. Additionally, it is expected that carboxylated CNTs could possibly react with the epoxy groups of GMA units in P(SSNa-*co*-GMA40), as described previously,[42] offering a more stable material with long lasting performance.

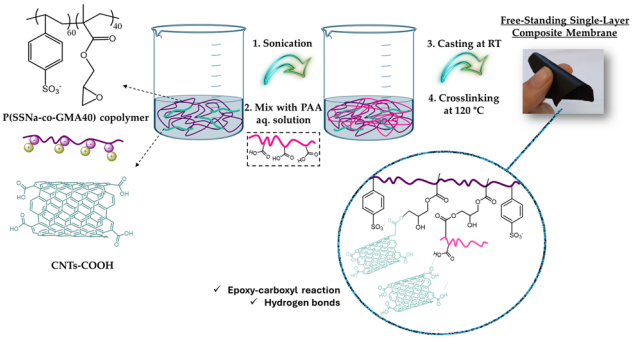

Fig. 1 Schematic illustration for the preparation of CNTs-polymer composite membranes.

To find the optimized conditions for the highest performance, composite membranes with four different contents of CNTs were prepared (5, 10, 20 and 30 wt%), as shown in Table S1, ESI.† These membranes, together with the neat membrane (0 wt% CNTs) were tested in terms of their stability in aqueous conditions through swelling and soluble fraction measurements. For this, two different treatment temperatures (room temperature and 120 °C) were used for membrane curing to study the cross-linking efficiency. As shown in Table S2, ESI† as CNTs loading increased, the membranes exhibited lower swelling ratios in both treatment temperatures, RT and 120 °C, due to the reduction of the overall hydrophilicity level of the membrane. In general, the values of swelling ratio after treatment at 120 °C are essentially lower than those at RT, revealing that the crosslinking reaction is favored at this temperature. This outcome is also reinforced from the soluble fraction measurements, where very low values are observed after crosslinking at 120 °C. Further evidence of the successful crosslinking reaction was provided by ATR-FTIR spectroscopy. As shown in Fig. S2 (ESI†), for the P(SSNa-*co*-GMA40)/PAA 90/10 w/w blend, the peak at 906 cm^{-1} attributed to the epoxy

ring of the GMA unit completely disappears after heat treatment of the membrane at 120 °C for 24 h. Thus, high temperature curing was selected for the preparation of the membranes in this work, since it favors the creation of robust materials that remain stable under high humidity levels.

Morphological characteristics of the composite membranes

The investigation of the composite single-layer membranes' morphology was conducted using high-resolution scanning electron microscopy (SEM). It is noticeable that the surface of the membranes with lower CNTs content (5–20%) is relatively smooth and there are no obvious micropores or hollows within the membrane (Fig. 2a–c) whereas when the percentage of nanotubes is higher (30% w/w) the surface shows a slight roughness (Fig. 2d). Fig. 2e–h show the cross-sectional morphology of the composite single-layer membranes. The SEM observation emphasizes that this polymeric system allows the incorporation of higher loadings of CNTs, as the uniform dispersion of the nanotubes within the polymer matrix is observed in all cases. It is noteworthy that the initial diameter of the nanotubes is 30–50 nm while after their incorporation into the mixture it increases significantly (120–140 nm) demonstrating a decoration of the CNTs structure with the polymeric materials. Another point worth mentioning is the morphological transformation that the membranes undergo following water swelling. To investigate this, membranes containing 10% and 30% nanotubes were immersed in water, allowed to swell, and subsequently subjected to lyophilization to preserve their expanded configuration. Fig. S3, ESI† reveals that these composite membranes gain a porous structure when exposed to a water environment. It is recognized that the presence of a porous structure confers improved actuation performance to the materials. This is attributed to its ability to increase the interfacial area between the material and air, as well as to provide a greater number of pathways for water absorption and desorption. Hence, this porous structure forming moisture transport channels offers the advantage of enhanced water molecule exchange with the surroundings allowing the composite film to exhibit improved sensitivity to changes in humidity level. The porous microstructure of the film, along with the presence of hydrophilic groups in the polymeric system allows for a highly responsive humidity behavior, as elaborated in a subsequent section.

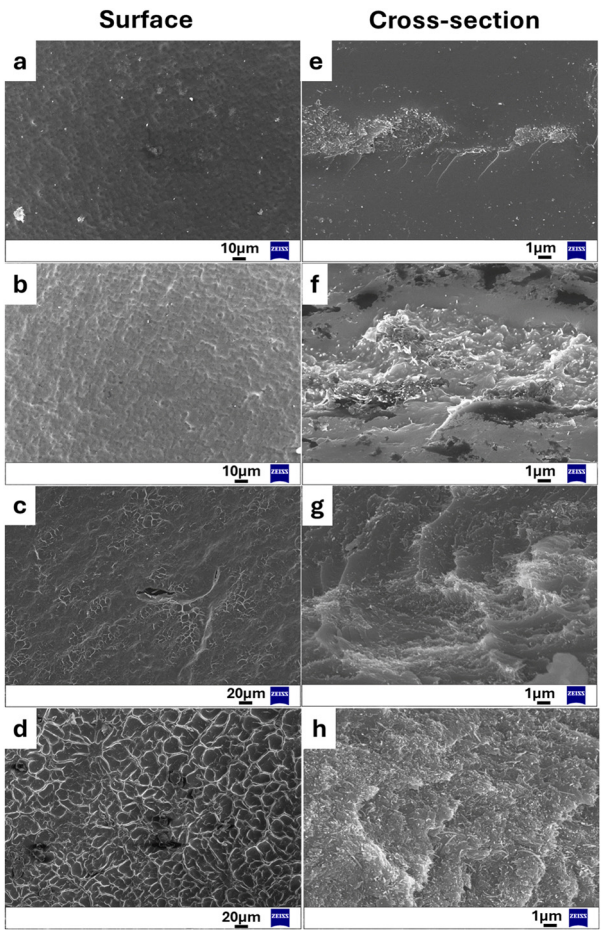

Fig. 2 Structural characterization of the composite membranes. SEM images of the surfaces (left) and the cross-section (right) of the cross-linked composite monolayer membranes with (a) and (e) 5% CNTs, (b) and (f) 10% CNTs, (c) and (g) 20% CNTs, (d) and (h) 30% CNTs.

Regarding surface properties of the prepared membranes, water contact angle measurements were employed to examine the influence of CNTs on surface wettability. As illustrated in Fig. S4 (ESI†), the contact angle values increase with a higher percentage of CNTs due to their inherent hydrophobic nature. However, at 30% CNTs loading, a slight decrease in the contact angle is observed. This occurs because the CNTs-COOH used in the composite membrane contain 0.7 wt% carboxyl content. At lower CNT loadings, the hydrophilic –COOH groups do not significantly impact the contact angles, allowing the hydrophobic nature of CNTs to prevail. Conversely, when the CNTs-COOH content exceeds 30%, the carboxyl groups introduce hydrophilicity to the membrane surface, resulting in a decreased contact angle. This reduction is further amplified by the increased surface roughness due to higher CNTs-COOH loadings.[26]

XRD analysis was also performed to determine the efficiency of the incorporation of CNTs into the polymeric matrix. The analysis was conducted for comparison purposes for both the different loadings of CNTs (5–30% w/w) and for the pure membrane without CNTs. The neat membrane displays a broad peak around a 2θ value of 17°, indicative of its amorphous nature. Considering Fig. S5 (ESI†), the peak at 2θ = 26° corresponds to the reflection (002) confirming the incorporation of CNTs.[26] As the CNTs increase, the peak at 2θ = 26° becomes more pronounced, particularly at a 30% CNTs loading.

Mechanical properties

Mechanical characterization of cross-linked membranes was performed by stress *vs.* strain measurements in tensile mode, evaluating Young's modulus (E), tensile yield strength (σ_b), and elongation at break (ε_b) (Fig. S6, ESI†). These properties are crucial for developing high-performance actuators/sensors for demanding applications. The neat P(SSNa-*co*-GMA40)/PAA

(0% CNTs) film shows the lowest tensile strength (21.5 ± 1 MPa) and Young's modulus (782 ± 21 MPa) compared to films with CNTs. As CNT loading increases (5, 10, 20, 30%), σ_b slightly decreases, but remains higher than the original membrane. Conversely, Young modulus (E) increases with higher CNT percentages as their inherent mechanical properties and their interaction with the polymer matrix.[30] These findings indicate that CNT reinforcement can significantly enhance the mechanical properties of composite membranes, making them suitable for various advanced applications.

Humidity-responsive studies

The purpose of this study was the development of humidity-sensitive membranes by incorporating partially-carboxylated multi-walled CNTs into a mixture of water-soluble copolymers. To assess the membranes' responsiveness to humidity, we measured the bending angle of narrow strip samples as they were exposed to a moist filter paper (as shown in Fig. 3).

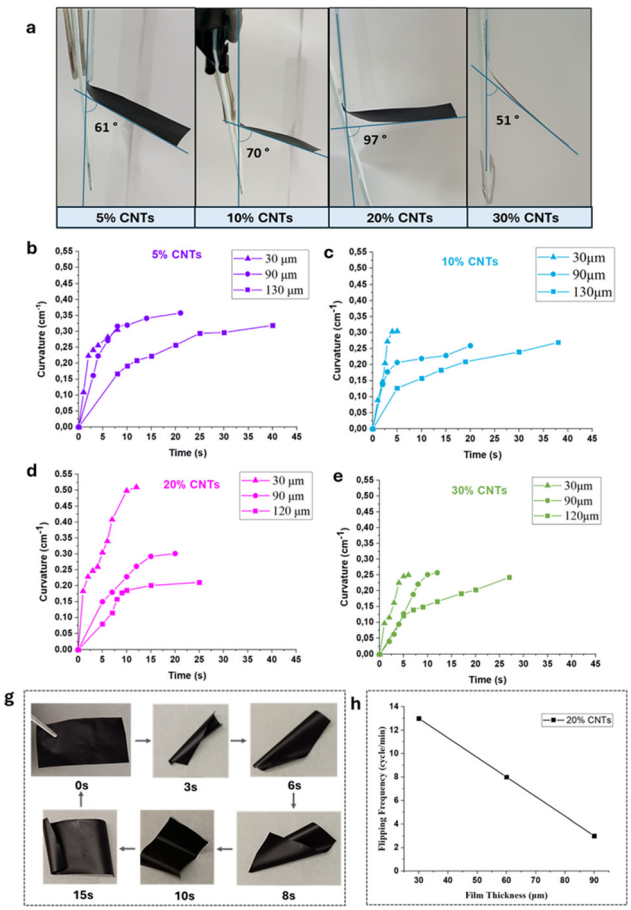

Fig. 3 Actuating performance of the composite membranes. (a) Photographs of the maximum bending deformations of narrow strip membranes showing their bending angles when approaching a wet filter paper. (b)–(e) The calculated curvature K (cm^{-1}) of the copolymer membranes, as a function of time for different CNTs contents and different thickness. (g) Photographs demonstrating the spontaneous locomotion of a rectangular film on a moist substrate. (h) Flipping frequency of the membranes with different thicknesses (30, 60 and 90 μm).

We captured photographs at the point where the bending angle was maximized for each membrane (Fig. 3a).

Surprisingly, these single-layer flexible membranes exhibited bending deformation mobility with an extremely fast response when exposed to a high moisture environment derived from a pre-wetted filter paper, as illustrated in Fig. 3a. The rectangular strips bend away from the moisture source and the curvature properties of the composite membranes were investigated as a function of time. This humidity-responsive behavior is assigned to an absorption/desorption mechanism of the membranes, by rapidly exchanging water molecules with the environment that's leads to film expansion and contraction. The induced swelling properties of these membranes, as displayed in Table S2, ESI† are facilitated by the strong hydrogen bonding interactions between the hydrophilic groups (–OH, –COOH, SO_3H) and the water molecules.[43] On the other hand, the presence of CNTs with their hollow nanochannels and inherent hydrophobic regions, may aid in the transportation and rapid desorption of the water molecules.

The degree of curvature, K (cm^{-1}) of the membrane strips was determined by the equation reported in the literature.[44] The calculated curvature values are presented in the form of graphs, as a function of time for different CNTs contents in the formed membranes and in different thicknesses as well (Fig. 3b–e). Interestingly, all samples showed fast response to moisture, with the curvature values varying between 0.25 and 0.35 cm^{-1}. Notably, membranes containing 20% CNTs exhibited significantly elevated curvature, exceeding 0.5 cm^{-1} when the membrane thickness is 30 μm. Understanding the relationship between curvature and thickness is crucial for designing humidity-responsive materials. Thicker membranes (90 and 120 μm) retain or expel water more effectively due to their increased mass and complexity, while thinner membranes (30 μm) respond faster to humidity changes, making them suitable for swift adjustments. As the thickness increases, the maximum bending angle gradually decreases, and the response/recovery time lengthens. This is likely because the composite film becomes stiffer, necessitating more driving power to overcome this increased stiffness, as noted in the literature.[25,26,41] Interestingly, the membranes showed excellent repeatability of their deformation after multiple exposures to the same humidity. As shown in Movie S1 (ESI†), the membrane performs 18 cycles for a period of 1 min, without noticeable fatigue, demonstrating the stability of the membrane's responsiveness to humidity over time.

Following with the humidity-responsive studies of the composite films constructed in this study, it was observed that rectangular-shaped membranes exhibited a locomotive cycle of six stages when placed on a damp surface, such as a pre-wetted filter paper (Fig. 3g and Movie S2, ESI†). This motility requires a water vapor gradient, as shown in similar studies.[41] Specifically, upon contact, the lower side of the film which is in contact with the moist substrate (higher humidity), immediately undergoes higher water-induced expansion than the side exposed to the air (lower humidity). As a result, the film initially

folds up to create a cylindrical structure and as the center of gravity shifts the film topples over leading to its upper surface to flip downward. Subsequently, the film bends from one corner, rolls horizontally and starts a new flipping cycle. The anisotropic swelling resulting from the *in situ* formation of a 'bilayer' structure drives the film to flip continually. When the film is removed from the moist substrate its motion halts instantly and can be resumed by placing it back on the moist paper. Notably, the thickness of the film affects the frequency of the flipping motion, as shown in the graph of Fig. 3h and in Movie S1, ESI† where three membranes of different thickness (30, 60 and 90 μm) were tested.

To showcase its mechanical capabilities, a rectangular membrane of 90 μm thickness and initial weight of 270 mg was loaded with small metal staples at its corners, functioning as external cargos, and was then positioned on a pre-wetted paper (Movies S3 and S4, ESI†). While introducing external cargo onto the membrane resulted in a noticeable change in the flipping frequency, it seemed that the membrane retains its capability of movement, even with a cargo of approximately double the weight of the membrane itself (130% additional weight) (Fig. 4a). From the graph of Fig. 4b, it can be seen that the flipping frequency decreases as the cargo's weight added on the membrane increases from 90 to 360 mg.

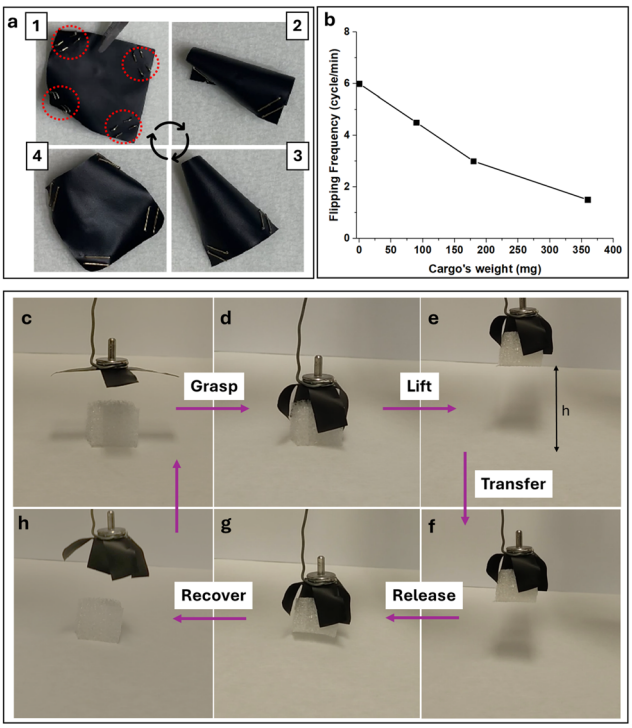

Fig. 4 Two examples of potential use of the membranes in the field of soft robotics. (a) Humidity-responsive membrane carrying a cargo of 360 mg. (b) Effect of cargo weight on flipping frequency (90, 180, 360 mg). Optical photos of the smart gripper that lifts a small object. (c) The initial state of the smart gripper at ambient humidity. (d)–(f) The gripper grasps and picks up the small object when in a high humidity environment. (g) and (h) The small object is released from the gripper when the humidity source is removed.

To further verify that moisture is the pivotal factor in this actuation performance of the composite membranes, two additional and simple experiments were conducted. Firstly, the membrane was placed on a bare hand and started flipping and folding motions, immediately upon contact with the normal moisture on the skin, as shown in Movie S5, ESI.† As anticipated though, when the hand was covered with a latex glove, the membrane remained still. Additionally, the same membranes were placed on filter papers wetted with three organic solvents of different polarity (ethanol, dimethylformamide and hexane). From the Movie S6, ESI† it can be realized that organic solvents do not trigger this unique performance of the composite membranes, except from ethanol, which seems to cause a very slight bending movement, probably due to its hydroxyl groups that may interact with the polymeric chains of the membrane through hydrogen-bonding. However, flipping or folding motions could not be achieved even in ethanol.

Aiming to use these materials in the field of soft robotics, a preliminary effort was made to design a smart gripper, using the composite membrane with 20% CNTs and thickness of 90 μm. The membrane was cut in a cross-shape and fixed on a metallic base. As shown in Fig. 4c–h, the 'claws' of the gripper bended under the stimulus of humidity, picking up successfully a cube-shaped foam. Movie S7, ESI† clearly shows all the stages of the process, where the membrane-gripper initially has the form of a cross and when high moisture flow is employed, the membrane-gripper deforms and grabs the foam, picks it up by and then releases it when the moisture flow stops, as the membrane-gripper recovers its initial state.

To gain a deeper understanding of the water absorption/desorption mechanism that causes the deformation of these materials, the composite membranes (90 μm) were immersed in D_2O for 10 seconds, then extracted and assayed utilizing ATR-FTIR spectroscopy.[44–46] ATR-FTIR spectra displayed in Fig. S7 (ESI†) depict the exchange of hydrogen (H) and deuterium (D) between the film and water vapors. The spectra are arranged from top to bottom, showing the initial membrane before immersion in D_2O, and then at 0, 1, 2, 3, 4, 5, 6 and 7 minutes after immersion in D_2O. When the film was exposed to D_2O, the intensity of the band at 2500 cm^{-1}, corresponding to the stretching vibration of O–D bonds, noticeably increased. Over time, the intensity of the peak at 2500 cm^{-1} decreased, indicating that the film exchanged water molecules with the surrounding environment (active protons in OH and COOH with deuterium atoms). At the same time, the rapid increase of the 3330 cm^{-1} band demonstrates the membrane's ability to efficiently and promptly absorb water from its surroundings, enabling a quick and reversible response to changes in environmental humidity. The impact of varying thickness of the composite membranes on humidity responsiveness was also investigated, through ATR-FTIR spectroscopy (Fig. S8, ESI†). Interestingly, the ATR spectra revealed that the higher thickness (120 μm) of the membrane resulted in a decreased rate of peak shifts, confirming that membrane thickness plays a role in influencing moisture responsiveness.

Conductivity measurements/applications of the CNTs composite membrane actuator/non-contact human–machine interface

We hypothesize that the composite membranes exhibit mixed conductivity, due to the incorporation of CNTs, that are known electrical conductors, and P(SSNa-*co*-GMA40) that exhibits ionic conductivity, due to its ionic nature. To have a clearer understanding of the mixed conductivity of the composite membranes, humidity sensors of different CNTs loadings were investigated in terms of their electrical properties. To correlate the humidity performance of the polymer/CNTs composites with their electrical characteristics, composites with different CNTs loadings were evaluated at different relative humidities, with a stable applied bias voltage of 1 V. The highest current flow is observed, as expected, for the composite with 30% CNTs loading, owing to the high electrical conductivity of the electrically active CNTs. It is notable that this composite, owing to the high percentage of CNTs, presents current flow (5.5×10^{-5} A) even at 0% RH, that is then reinforced by introduction of the ionization effect. This finding further reinforces our initial hypothesis that these composite membranes present mixed conductivity. At 75% RH the composites with 30% CNTs present the highest value of current flow, at about 3×10^{-4} A, while at higher RHs, current flow reduces, probably due to saturation of the membranes. Next, the composite with 20% CNTs also displays high mixed conductivity, starting even from relatively low humidities of 11%. Then, with increasing RH, a maximum current of 1.1×10^{-4} A is reached for 95% RH (Fig. 5a). These conductivity values are encouraging for further applications of the composite membranes with 20% and 30% CNTs, since they are relatively high, when compared with similar composites[47] and they also require small loading of CNTs to achieve high conductivity.[26,30] In the case of 5% and 10% CNTs loading (Fig. 5b), the composites still present mixed conductivity, albeit at lower values, reaching a maximum 7×10^{-7} A for the composite with 10% CNTs. It is notable that in all cases, the composites' conductivity has a low threshold of 11% RH, at which point they act as electrical conductors, pointing to relatively high humidity sensitivity. It is also worth noting that regardless of the CNTs loading, all composites behave as n-type conductors, as with increasing humidity all composites have increasing current flow. From these findings it is concluded that composites with loadings higher than 10% can be considered for humidity sensing applications.

The *I–V* characteristics of the polymer/CNTs composites were also obtained (Fig. 5c), where with increasing CNTs loading, the composites exhibit increasing flow of current. The linear relationship between applied voltage and current points to a typical ohmic characteristic for all prepared composites. These results, obtained at ambient relative humidity, confirm the conductivity of the composites, especially at 10–30% CNTs loading.

The in-plane conductivity of the composite membranes was measured using the four-point probe method and revealed a steady increase with rising CNT percentage in the membranes. While for the neat membranes and for 5% loading, the conductivity was very low (σ = 0.01 S m^{-1}), revealing a more insulating nature for the membranes, by raising the CNT percentage the conductivity showed a marked increase of two orders of magnitude (σ = 1.01 S m^{-1} for 10% loading, and σ = 10.58 S m^{-1} for 20% loading). The highest value was reached as was expected for 30% CNT percentage, where the membranes showed a high value of 200 S m^{-1} (Fig. 5d).

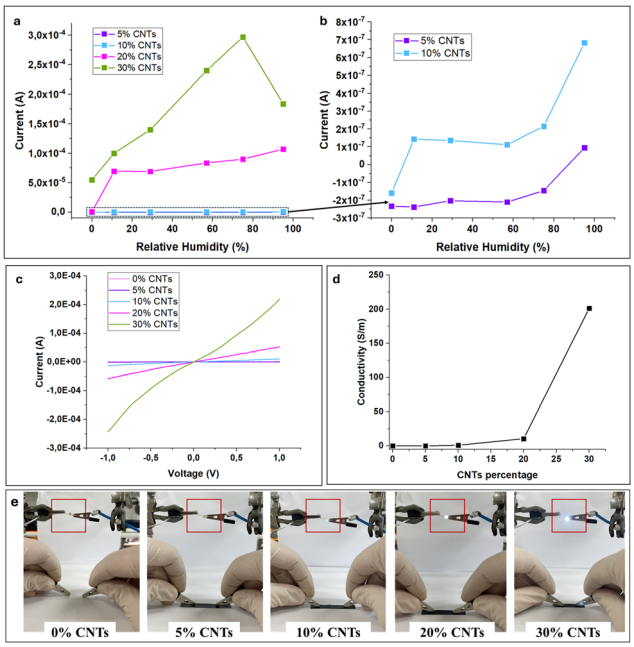

Fig. 5 Electrochemical characterization of the composite membranes and demonstration of their conductivity. (a) Current flow for the composite membranes at a range of different RHs. (b) Current flow of the composite membranes with 5%, 10% CNTs at different RHs. (c) *I–V* characteristics of the composite membranes with 0–30% CNTs. (d) In-plane conductivity measurements of the composite membranes with 0–30% CNTs. (e) The images demonstrate that the LEDs remained unlit when connected to the circuit, with a membrane 0% CNTs and 5% CNTs indicating the high resistance of the films. When the LED was attached in the 10% CNTs, 20% CNTs and 30% CNTs circuit emitted a rising brighter light with the increase of CNTs content.

The conductivity of the as-prepared sensors based on the composites, has also been visually confirmed by the turn-on of an LED, connected to the sensors. As illustrated in Fig. 5e, the electrical conductivity of the composite membrane is influenced by the CNTs content. The presence of CNTs leads to a notable increase in electrical conductivity, which is evident from the brightness of the LED illuminated by the composite films. As expected, for lower CNT content the LED does not turn on, as the composites possess high impedance. By raising the CNT content, however, the conducting nature of the composites can clearly be observed.

The impedance of the composite membranes with 1%, 10% and 38% CNTs loading was also measured. The membranes were measured in dry and wet states, to pinpoint differences in their conductivities throughout their Bode plots spectra. For 1% loading, only the dry films were measured, as in this case we were not able to measure the wet films. For these dry films,

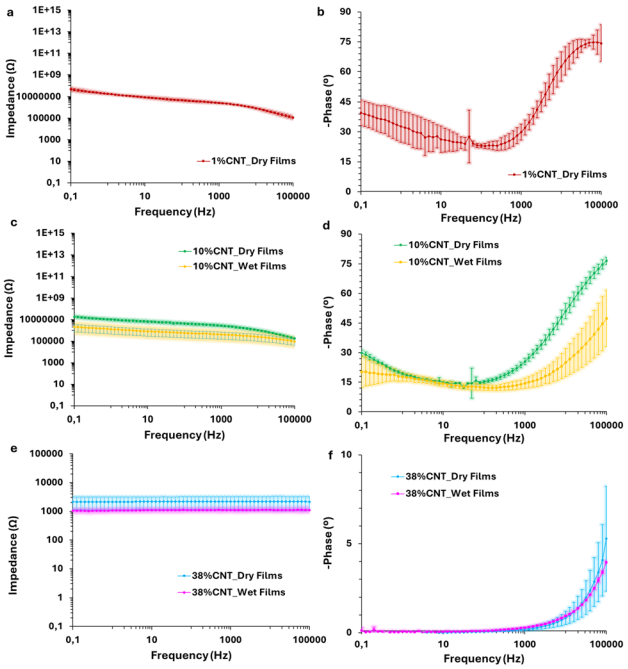

Fig. 6 Electrochemical Impedance Spectroscopy of wet and dry membranes. Impedance bode plot spectra (a), (c) and (e) of the composite membranes with 1%, 10% and 38% CNTs loading in their dry and wet states. Phase diagrams *versus* frequency for the same films (b), (d) and (f).

an impedance of about $4.8 \pm 1.2 \times 10^7$ Ω was measured at 0.1 Hz (Fig. 6a). We can hypothesize that 1% CNT was insufficient to reach an electronic percolation threshold that allows electron charge movement throughout the sp^2 carbon atoms of the carbon nanotubes. Indeed, a capacitive effect is observed at low frequencies (0.1 Hz) with a phase of $-39.6 \pm 6.3°$. This is probably due to the ionic conduction nature of the sodium styrene sulfonate and the high percentage (99%) of the copolymer within the film (Fig. 6b). For 10% loading, the impedance of the films shows a marked decrease of about two orders of magnitude, *i.e.* $18.6 \pm 4.2 \times 10^6$ Ω and $2.11 \pm 1.4 \times 10^6$ Ω for dry and wet states respectively at 0.1 Hz (Fig. 6c). The difference in the impedance between the dry and wet states is smaller, as the conductivity of the films is largely affected by the presence of the CNTs in the composite membranes. In addition, a similar trend can also be observed from their phase diagrams *i.e.* -29.9 ± 1.5 and $-20.1 \pm 7.9°$ for dry and wet films, respectively (Fig. 6d). On the opposite to 1% CNT wet films, the phase of 10% CNT wet films tend to 0°, indicating a more resistive behavior. Lastly, 38% CNT films present impedances some order of magnitudes lower than the previous studied films (2.1 ± 0.9 and $1.0 \pm 0.031 \times 10^3$ Ω for dry and wet respectively at 0.1 Hz). The dry and wet states show even less difference, reinforcing the assumption that their conductivity is largely affected by the CNTs loading. Moreover, 38% CNT films have a behavior that is purely resistive, denoted as the plateau value along the different frequencies. This is corroborated by the phase, which stays close to 0° in the whole range of frequencies.

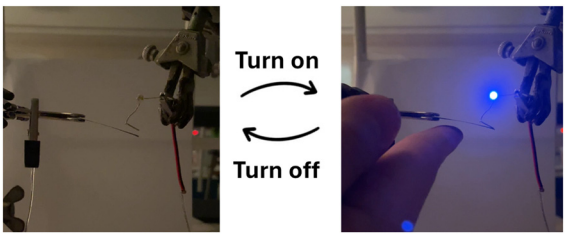

Fig. 7 Non-contact human–machine interface. Images of the smart non-contact switch, which activates or deactivates the circuit in response to variations in humidity (snapshots from Movie S8, ESI†).

In order to also take advantage of the humidity-responsive actuation of our membranes, however, we also demonstrate their ability to be used as smart, humidity-driven switches (Fig. 7; Movies S8 and S9, ESI†). Upon exposure to moisture as a finger approached, the composite film bent upwards and away from the finger, coming in contact with the electrode of the LED, turning it on in the process. When the finger was pulled away and the humidity in the composite membrane reached ambient again, the membrane returned to its original position, switching off the LED. Both membranes with 20% and 30% CNTs content that were tested functioned efficiently as smart switches, as shown in Movies S8 and S9, ESI,† respectively. These experiments clearly demonstrate the potential of our composite membranes as conductive humidity-driven smart switches.

Even though the membrane with 30% CNTs displayed the highest conductivity, when considering applications such as humidity sensors or non-contact switches, additional properties must be taken into consideration, such as bending angle, curvature of the deformation and mechanical properties. As shown earlier, the membrane with 30% CNTs shows smaller bending angle than its 20% counterpart, along with a smaller strain at break. For these reasons the membrane with 20% CNTs seems to be the most versatile, to be considered for a range of applications based on its humidity-responsiveness, its mechanical performance and its conductivity.

The ability of the membranes to act as moisture-driven generators can also be demonstrated. The mechanism of power

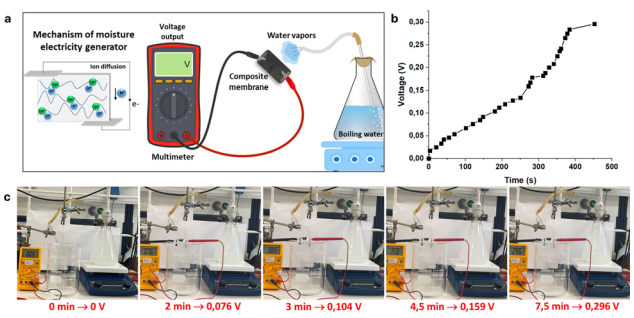

Fig. 8 Moisture-induced electricity generation. (a) Illustration of the output voltage generated by the film under continuous water vapors. (b) Continuous voltage output from a piece of a composite membrane, (c) evolution of the output voltage generated by the film under continuous water vapors.

generation relies on the directional transmission of protons induced by the ionization effect within the composite films due to the humidity gradient. Specifically, as the environmental humidity gradually rises, the abundant carboxyl groups in the composite membranes dissociate, resulting in the generation of more mobile protons. This proton gradient on both sides of the film (as illustrated in Fig. 8a) drives the power generation process (as shown in Fig. 8b). The film's output voltage demonstrates a continuous increase with ongoing humidification, eventually reaching 296 mV after 7.5 minutes (Fig. 8c).

Conclusions

In summary, a facile and environmentally friendly methodology was employed to fabricate composite membranes with dual conductivity and humidity-induced mobility. These novel membranes are formed through the crosslinking of the water-soluble copolymer P(SSNa-*co*-GMA40) and carboxyl groups derived from acrylic acid and partially-carboxylated carbon nanotubes. Single-layer membranes with varying levels of CNTs demonstrate ionic conductivity under moist conditions, while their electronic conductivity rises in correlation with the amount of CNTs present, reaching up to 200 S m^{-1} for 30% CNTs loading. Remarkably, these membranes also demonstrate rapid responsiveness to humidity changes. Detailed investigations reveal that these flexible single-layer membranes exhibit bending, flipping, and folding motions instantly when exposed to high humidity environments, with potential applications in the fields of smart sensing devices and soft robotics. Moreover, these composite membranes can serve as non-contact switches and most interestingly may even find application in the field of hygroelectric generators, since preliminary results showed an output voltage of about 300 mV upon continuous humidity transfer. Thus, these findings create new dimensions for investigation of advanced materials with a wide range of applications.

Experimental section/methods

A detailed description of the materials and methods used in our experiments and models is provided as ESI.†

Data availability

The data supporting this article have been included as part of the ESI.†

Author contributions

I. T. contributed to all experimental parts of the synthesis, characterization, and analysis. D. D. contributed to the experiments related to the humidity responsiveness of the membranes. K. C. A. performed the electrochemical characterization of the membranes and analyzed results. A. D. A. and G. G. M. performed and analyzed the through plane EIS measurements. J. K. K. supervised the research and reviewed the manuscript. I. T. and D. D. designed and wrote the main manuscript text, and K. C. A., A. D. A., G. G. M., contributed to specific sections. All authors have given approval to the final version of the manuscript.

Conflicts of interest

There are no conflicts to declare.

Acknowledgements

Dr Vassilios Drakopoulos from the Institute of Chemical Engineering Sciences (ICE/HT-FORTH) is acknowledged for the SEM/EDX characterizations.

Notes and references

1 Q. Zheng, C. Xu, Z. Jiang, M. Zhu, C. Chen and F. Fu, *Front. Chem.*, 2021, **9**, 650358.
2 M. Li, A. Pal, A. Aghakhani, A. Pena-Francesch and M. Sitti, *Nat. Rev. Mater.*, 2022, **7**, 235–249.
3 Y. Lu, G. Yang, Y. Shen, H. Yang and K. Xu, *Nano-Micro Lett.*, 2022, **14**, 150.
4 L. Zhang, H. Liang, J. Jacob and P. Naumov, *Nat. Commun.*, 2015, **6**, 7429.
5 G. Jia, A. Zheng, X. Wang, L. Zhang, L. Li, C. Li, Y. Zhang and L. Cao, *Sens. Actuators, B*, 2021, **346**, 130507.
6 N. El-Atab, R. B. Mishra, F. Al-Modaf, L. Joharji, A. A. Alsharif, H. Alamoudi, M. Diaz, N. Qaiser and M. M. Hussain, *Adv. Intell. Syst.*, 2020, **2**, 2000128.
7 C. Hegde, J. Su, J. M. R. Tan, K. He, X. Chen and S. Magdassi, *ACS Nano*, 2023, **17**, 15277–15307.
8 Y. Dong, J. Wang, X. Guo, S. Yang, M. O. Ozen, P. Chen, X. Liu, W. Du, F. Xiao, U. Demirci and B.-F. Liu, *Nat. Commun.*, 2019, **10**, 4087.
9 W. A. D. M. Jayathilaka, K. Qi, Y. Qin, A. Chinnappan, W. Serrano-García, C. Baskar, H. Wang, J. He, S. Cui, S. W. Thomas and S. Ramakrishna, *Adv. Mater.*, 2018, **31**, 1805921.
10 G. Agarwal, N. Besuchet, B. Audergon and J. Paik, *Sci. Rep.*, 2016, **6**, 34224.
11 J. Lee, M. W. M. Tan, K. Parida, G. Thangavel, S. A. Park, T. Park and P. S. Lee, *Adv. Mater.*, 2020, **32**, 1906679.
12 H. S. Kim, J. H. Kang, J. Y. Hwang and U. S. Shin, *Nano Convergence*, 2022, **9**, 35.
13 Z. Wu, Q. Ding, H. Wang, J. Ye, Y. Luo, J. Yu, R. Zhan, H. Zhang, K. Tao, C. Liu and J. Wu, *Adv. Funct. Mater.*, 2024, **34**, 2308280.
14 Y. Liang, Z. Wu, Y. Wei, Q. Ding, M. Zilberman, K. Tao, X. Xie and J. Wu, *Nano-Micro Lett.*, 2022, **14**, 52.
15 X. Liu, D. Zhang, D. Wang, T. Li, X. Song and Z. Kang, *J. Mater. Chem. A*, 2021, **9**, 14524.
16 J. Wu, Y. M. Sun, Z. Wu, X. Li, N. Wang, K. Tao and G. P. Wang, *ACS Appl. Mater. Interfaces*, 2019, **11**, 4242–4251.

17 Z. Duan, Y. Jiang, M. Yan, S. Wang, Z. Yuan, Q. Zhao, P. Sun, G. Xie, X. Du and H. Tai, *ACS Appl. Mater. Interfaces*, 2019, **11**, 21840–21849.
18 T. Li, L. Li, H. Sun, Y. Xu, X. Wang, H. Luo, Z. Liu and T. Zhang, *Adv. Sci.*, 2017, **4**, 1600404.
19 J. Yang, R. Shi, Z. Lou, R. Chai, K. Jiang and G. Guozhen Shen, *Small*, 2019, **15**, 1902801.
20 P. Guan, R. Zhu, G. Hu, R. Patterson, F. Chen, C. Liu, S. Zhang, Z. Feng, Y. Jiang, T. Wan, L. Hu, M. Li, Z. Xu, H. Xu, Z. Han and D. Chu, *Small*, 2022, **18**, 2204603.
21 J. He, P. Xiao, J. Zhang, Z. Liu, W. Wang, L. Qu, Q. Ouyang, X. Wang, Y. Chen and T. Chen, *Adv. Mater. Interfaces*, 2016, **3**, 1600169.
22 W. Pu, F. Wei, L. Yao and S. Xie, *J. Mater. Sci.*, 2022, **57**, 12202–12235.
23 S. Ding, T. Yin, S. Zhang, D. Yang, H. Zhou, S. Guo, Q. Li, Y. Wang, Y. Yang, B. Peng, R. Yang and Z. Jiang, *Langmuir*, 2023, **39**, 1474–1481.
24 P. Zhou, L. Chen, L. Yao, M. Weng and W. Zhang, *Nanoscale*, 2018, **10**, 8422.
25 Q. Chen, X. Yan, H. Lu, N. Zhang and M. Ma, *ACS Appl. Mater. Interfaces*, 2019, **11**, 20473–20481.
26 J. Wei, S. Jia, J. Guan, C. Ma and Z. Shao, *ACS Appl. Mater. Interfaces*, 2021, **13**, 54417–54427.
27 J. Mu, C. Hou, B. Zhu, H. Wang, Y. Li and Q. Zhang, *Sci. Rep.*, 2015, **5**, 9503.
28 H. Chen, Y. Ge, S. Ye, Z. Zhu, Y. Tu, D. Ge, Z. Xu, W. Chen and X. Yang, *Nanoscale*, 2020, **12**, 6104–6110.
29 V. Datsyuk, M. Kalyva, K. Papagelis, J. Parthenios, D. Tasis, A. Siokou, I. Kallitsis and C. Galiotis, *Carbon*, 2008, **46**, 833–840.
30 P. Shen, Z. Jiang, J. Viktorova, B. Pollard, A. Kumar, Z. Stachurski and L. A. Connal, *ACS Appl. Nano Mater.*, 2023, **6**, 986–994.
31 X. Peng, J. Chu, A. Aldalbahi, M. Rivera, L. Wang, S. Duan and P. Feng, *Appl. Surf. Sci.*, 2016, **387**, 149–154.
32 T. Fei, K. Jiang, F. Jiang, R. Mu and T. Zhang, *J. Appl. Polym. Sci.*, 2014, **131**, 39726.
33 S. Pyo, Y. Eun, J. Sim, K. Kim and J. Choi, *Micro-Nano Syst. Lett.*, 2022, **10**, 9.
34 G. Zhou, J. H. Byun, Y. Oh, B. M. Jung, H. J. Cha, D. G. Seong, M. K. Um, S. Hyun and T. W. Chou, *ACS Appl. Mater. Interfaces*, 2017, **9**, 4788.
35 Z. Li, J. Wang, L. Dai, X. Sun, M. An, C. Duan, J. Li and Y. Ni, *ACS Appl. Mater. Interfaces*, 2020, **12**, 55205–55214.
36 J. M. Tulliani, B. Inserra and D. Ziegler, *Micromachines*, 2019, **10**, 232.
37 Q. Wei, W. Ge, Z. Yuan, S. Wang, C. Lu, S. Feng, L. Zhao and Y. Liu, *Nano Res.*, 2023, **16**, 7496–7510.
38 Y. Huang, H. Cheng, C. Yang, P. Zhang, Q. Liao, H. Yao, G. Shi and L. Qu, *Nat. Commun.*, 2018, **9**, 4166.
39 P. Li, N. Su, Z. Wang and J. Qiu, *ACS Nano*, 2021, **15**, 16811–16818.
40 D. Druvari, N. D. Koromilas, G. Ch Lainioti, G. Bokias, G. Vasilopoulos, A. Vantarakis, I. Baras, N. Dourala and J. K. Kallitsis, *ACS Appl. Mater. Interfaces*, 2016, **8**, 35593–35605.
41 D. Druvari, F. Kyriakopoulou, G. C. Lainioti, A. Vlamis and J. K. Kallitsis, *ACS Appl. Mater. Interfaces*, 2023, **15**, 11193–11207.
42 G. C. Lainioti, G. Bounos, G. A. Voyiatzis and J. K. Kallitsis, *Polymers*, 2016, **8**, 190.
43 J. Shen, A. Liu, Y. Tu, G. Foo, C. Yeo, M. B. Chan-Park, R. Jiang and Y. Chen, *Energy Environ. Sci.*, 2011, **4**, 4220–4229.
44 Z. Zhao, Y. Hwang, Y. Yang, T. Fan, J. Song, S. Suresh and N. J. Cho, *Proc. Natl. Acad. Sci. U. S. A.*, 2020, **117**, 8711–8718.
45 M. Ma, L. Guo, D. G. Anderson and R. Langer, *Science*, 2013, **339**, 182–186.
46 Y. Zhu, J. Zhang, Q. Wu, M. Chen, G. Huang, J. Zheng and J. Wu, *ACS Appl. Mater. Interfaces*, 2020, **12**, 15757–15764.
47 P. Zhu, Y. Liu, Z. Fang, Y. Kuang, Y. Zhang, C. Peng and G. Chen, *Langmuir*, 2019, **35**, 4834–4842.

